ORIGINAL ARTICLE

Effect of short basalt fibers on energy-dissipating properties of lightweight rubberized concrete shear wall

Artem Zaitsev[a*], Evgenii Matiushin[b], Victoria Shvetsova[b], Alexander Burukhin[a], Stepan Konev[a], Radmir Karamov[a], Ivan Sergeichev[a]

[a] Skolkovo Institute of Science and Technology, Moscow – 121205, Russia.
[b] Moscow State University of Civil Engineering, Moscow – 129337, Russia.
*Corresponding Author: Artem Zaitsev. Email: artem.zaitsev@skoltech.ru.

Abstract: To enhance the dynamic performance of shear walls, fine-grained rubberized basalt fiber concrete has been proposed as an alternative to conventional concrete. This is a promising material, yet the existing literature lacks an in-depth analysis of its energy dissipation properties. A comprehensive study was performed of fine-grained 100 x 100 mm cylindrical rubberized concrete specimens, both with and without basalt fibers, under low-cycle compression fatigue. The first concrete mixture had a volume fraction of 10 % crumb rubber, and the second concrete mixture contained a volume fraction of 0.3 % basalt fiber in addition to 10% crumb rubber. Scanning electron microscopy and computer tomography were used to validate the material's inner structure, adhesion, crumb rubber and basalt fiber distribution. To acquire the mechanical and dynamic properties of the material, hysteresis loops were obtained from 1000 cycles of compression fatigue tests under 0.1 and 0.05 strain rates on a servo-hydraulic machine through quasi-static laboratory tests. The obtained concrete properties were incorporated into VUMAT plasticity model of concrete and imported to ABAQUS for seismic analysis of reinforced concrete shear walls. A cyclic pushover analysis of the shear wall has been conducted to characterize its hysteretic behavior and energy dissipation for two consecutive concrete series, predicting long-term seismic performance. The concrete series with basalt fiber exhibited higher seismic resilience with hysteretic damping of 9.3% compared to 8.7% for the series without basalt fibers.

Keywords: Lightweight reinforced concrete shear wall; seismic resilience; energy dissipation; dynamic performance optimization; rubberized basalt fiber concrete; cyclic pushover analysis

1 Introduction

For reinforced concrete (RC) shear walls to have adequate strength, high stiffness, high bearing capacity, and sufficient ductility to prevent brittle shear failures, they need to be acutely designed [1,2]. Because of inadequate material and structural design, shear walls are experiencing damage from seismic events all over the world. To achieve a seismic resilient design, sustainable materials with viable mechanical and dynamical properties need to be further investigated. Fine-grained (lightweight) rubberized concrete (RuC) has recently received much interest in the earthquake engineering and sustainability sectors as a sustainable alternative. It is characterized by a low elasticity modulus, high damping, high energy dissipation, considerable deformation capacity, and good crack resistance [3–12].

According to various research results, rubber from waste tires can be used to replace part of the natural aggregates, such as sand or gravel in conventional concrete, resulting in a product called rubberized concrete [6,7,13–15]. Crumb rubber (CR) particles are in the range of 2 to 10 mm and are used to replace fine or coarse aggregate [3,5,15,16]. RuC can improve energy dissipation, ductility and damping ratio, which are paramount parameters in earthquake-resistant construction of concrete structures with the design requirement to withstand high impact seismic vibrations [5,13–15,17]. Manufacturing of RuC can enhance energy absorption of the traditional concrete under seismic load and, as a result, grant additional tensile strength at the same time [14,18]. However, because rubber has a poor bonding adhesion, it will decrease the concrete's density and compressive strength, respectively. Therefore, to address this shortcoming, modifications to the RuC mixture design are required.

Crumb rubber is supreme as it increases the strength of concrete in comparison to other forms of rubber, and the percentage of rubber replaced also affects the strength of concrete [14]. Up to a certain amount, adding CR can considerably improve concrete's energy absorption and impact resistance while preserving its other mechanical properties [6,13–16]. However, rubber increases the tensile strength of concrete, it decreases its compressive strength. To overcome this flaw, basalt fibers (BF) may be added to concrete mixture. Basalt fiber demonstrates promising results for compressive strength improvement as well as a higher tensile strength than E-glass fibers. On average, it is 2.5 times stronger than steel fibers and possesses a few distinguishing qualities of fire, acid and alkaline resistance [8–11,17,18].

It is indicated by various researchers that the addition of a small volume of basalt fibers increases the ductility and toughness of concrete structures [8–11,18]. Nevertheless, the fibers are able to sustain a specific load bearing capacity following the addition of a specific volume of basalt fibers and after matrix cracking, preventing an abrupt failure of the concrete material [17–19]. Furthermore, it has been tested that the crack widths are smaller than those of regular concrete [8,17,18]. In addition, basalt fibers in a concrete mixture provide moisture resistance and evenly distributes temperature extremes more effectively than steel or plastic fiber reinforcement. Contemporary studies are mainly focused on investigation of the mechanical properties of basalt fiber reinforced concrete, and the data for energy-dissipation in the domain of dynamic properties of basalt fiber rubberized concrete is lacking.

Investigating the stiffness degradation and subsequent damage to a specimen that results from the coalescence of voids and microcracks within the material at the interface between cement paste and aggregates is crucial when designing an earthquake-resistant concrete material [20]. Material micro-structural changes are caused by hysteretic damping in the initiation stage of cyclic loading following the change of mechanical, energy-dissipating properties and stress response in the material [10,11,21]. When subjected to seismic excitation, there is an appearance of hysteretic effect and it relates to energy dissipation mechanism of a specimen response with the characteristic increase of resistance against material deformation under cyclic loading [22]. Its intensity usually decreases with a number of cycles until fatigue failure has occurred [21,23]. Within the framework of the theory of plasticity, the dependence of the stresses on the history of the material and their interaction, plastic deformation and proceeding degradation can be described by means of internal variables, such that would correspond to hysteretic (internal) damping.

When applying the designed concrete material to seismic finite element simulations of the shear wall, the best approach needs to be adapted to acutely simulate the structural behaviour under seismic excitation. For such non-linear calculations of structures, as Pushover analysis, there is a need to define a damping matrix. Several kinds of methods, such as viscous or hysteretic, can be used for that purpose [21,24]. However, a more viable approach should consist of a better modeling of the internal energy dissipation, whose introduction can be made at the material (specimen) level. State-of-the-art experiments on reinforced concrete subjected to seismic loading have shown a strong relationship between the state of failure and the consequent global damping [21–23,25,26]. Most of the damage plasticity models can acutely calculate those non-linear trends with the extension in the static case. However, when concrete still exhibits energy dissipation because of frictional sliding between crack lips at a certain damage level, these models ignore a cyclic feature of the residual hysteresis loop. [21,22,26]. Hence, an improvement of the material model is required for a better modeling of this dissipative part of structural behaviour. The modeling of such features provides a more physical means of taking damping into account without using any Rayleigh-type damping matrix. To undertake a non-

linear response of structures under high intensity earthquakes, it is necessary to establish a reasonable mechanical model for RC solid shear wall that takes into account the residual hysteresis loop and energy dissipation mechanism.

Although prior research in the field has identified positive application of rubberized concrete (RuC), the effect of adding basalt fibers on energy-dissipating properties of fine-grained RuC has not been investigated in full. This research aims to investigate energy-dissipation behavior of RuC with and without basalt fibers. This will add on the existing data and will help to understand the effect of using this concrete material in earthquake-resistant construction. To achieve high computational power for seismic simulations, we have built a Vectorized User Material (VUMAT) plasticity model of concrete to acutely capture its hysteretic behaviour and energy dissipation mechanism when subjected to low-cyclic fatigue. VUMAT utilizes vectorized programming techniques that take advantage of parallel processing capabilities, making it efficient for multicore CPUs, resulting in reduced computation times. This enables VUMAT to achieve significant speed improvements over UMAT and Concrete Damage Plasticity model, especially for such large-scale simulations as shear wall involving a wide array of material nodes.

Thus, our findings will allow to evaluate a potential application of lightweight basalt fiber rubberized concrete in the design of shear wall, and understand the mechanism of rubberized concrete' energy-dissipation. Investigating the effect of adding BF to a fine-grained rubberized concrete on its energy-dissipation properties, can not only add more data on the material, but can also potentially yield a seismically-resilient and sustainable material.

2 Materials

2.1 Specimen Fabrication

The concrete mixture has been designed for a fine-grained type of concrete with two series of mixtures: series **CR** – with the 10 % volume fraction of crumb rubber and series **CRBF** - with the 10 % volume fraction of crumb rubber and 0.3 % of basalt fibers. A 10% volume fraction of CR was chosen in accordance with research conducted by [4,5,13–15] as this volume fraction provided an optimum ratio between compressive strength and tension increase with a moderate rate of compressive strength decrease. A 0.3% volume fraction of BF was chosen per [10,11] as the volume fraction between 0.25-0.3 yielded the best compressive and tensile strength for concrete specimens. The length of BF is 12 mm and the diameter of BF is 14-16 μm. The diameter of CR is 2-4 mm. A concrete mixture for each series is reflected in **Table 1**.

Table 1. Concrete Mixture Composition

Series	CR		CRBF	
Component	Mass, kg	Volume, m^3	Mass, kg	Volume, m^3
Portland Cement	590	0.199	590	0.199
Water	255	0.255	255	0.255
Sand	1181	0.446	1180	0.444
Crumb Rubber	110	0.100	110	0.100
Basalt Fiber	0	0	3.9	0.0015

After designing a concrete mixture, the required quantity of raw materials (water, cement, sand, crumb rubber) is measured using scales. Sand and crumb rubber were dried beforehand. Their moisture content was equal to 0%. The temperature of all raw materials was in the range of 23±1 °C. The mixer bowl and blades were cleaned beforehand. Sand, cement, crumb rubber were added to the mixer bowl and mixed without adding water for 30 seconds. Then 2/3 of the mixing water was added to the mixer and the resulting concrete mixture was mixed for 1.5 minutes. The remaining water was mixed with Plasticizer and added to the concrete mix. The concrete mixture was then mixed for another 1.5 minutes.

Before pouring the concrete mixture, the cylinder moulds were pre-treated internally with Sika Separol-415 F grease. The moulds were then filled with concrete mixture in 2 layers; each layer was bayoneted with a cylinder cement bayonet 25 times. After the moulds were completely filled with concrete mix, the moulds were vibrated for 20 seconds. Excess concrete mix was cut off with a ruler.

The specimens were placed to the curing cabinet. After 1 day, the specimens were taken out of the cabinet, demoulded and returned to the cabinet again for another 27 days.

Following the moulding process, the specimens were kept in a laboratory setting at +20 ℃ for a full day. The exposed surface of the specimens was covered with polyethylene film to prevent moisture evaporation. After 24 hours, the specimens were removed from the mould and stored for the next 27 days at +20 °C and relative humidity of 100%. Before testing, the surfaces of the samples were carefully grinded.

The process of making concrete mixture with fibers (series CRBF) is similar except for one point: when the concrete mix is ready, basalt fiber is manually added to it in portions. After adding the entire proportion of fibers, the concrete mixture is additionally mixed for 1 minute. The concrete cylindrical specimens with the dimensions of CR and BF are shown in **Fig. 1.**
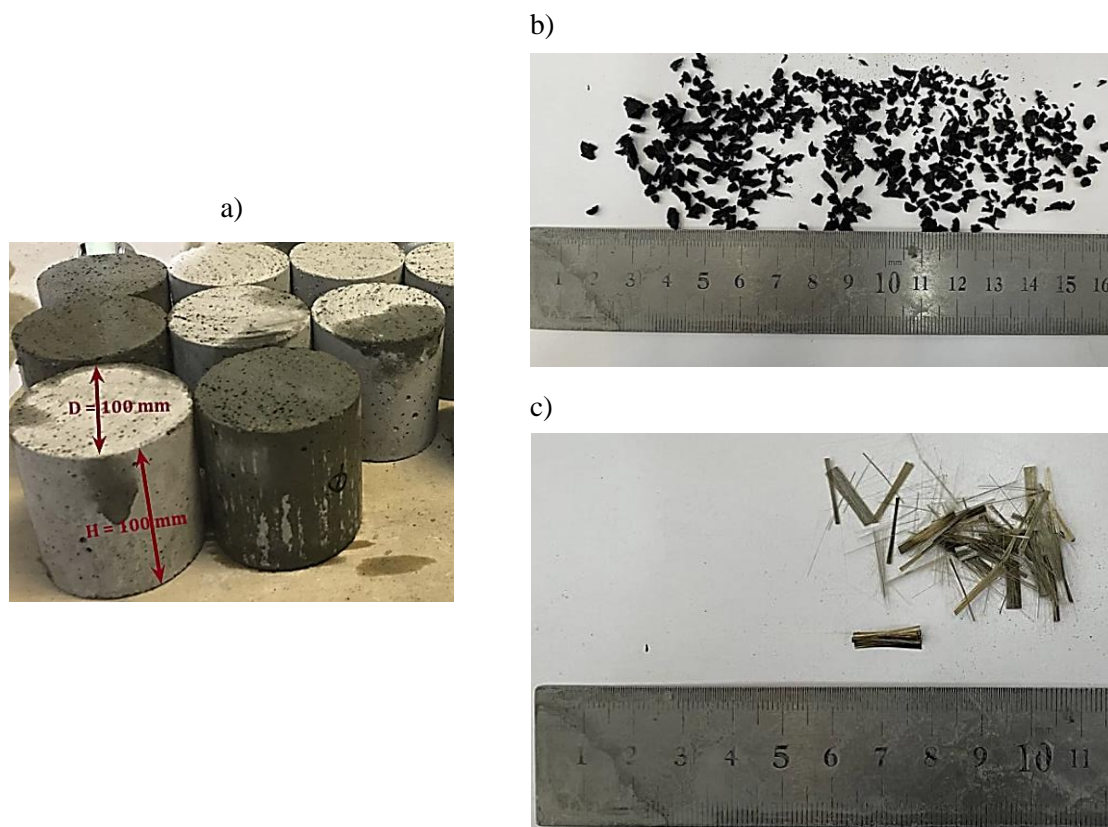

Fig. 1. Dimensions of concrete specimen and its compound: a) Concrete; b) CR (2-4 mm); c) BF (12 mm).

A total number of 24 specimens were prepared. To determine Elasticity modulus and Poisson's ratio, three specimens for each series were used for uniaxial compression. The rest 9 specimens for each series were used for low-cycle fatigue experiments. An overview for the testing setup is presented in the table below.

Table 2. Testing setup

Material mixture series (Total N of specimens)	N of specimens for uniaxial compression	N of specimens for low-cycle fatigue testing
CR (12)	3	9
CRBF (12)	3	9

2 2 Material Characterization

Scanning Electron Microscopy (SEM) and X-Ray computed tomography were performed to investigate the material's inner structure. For the image processing, ImageJ software was used. SEM probes were taken from the upper and lower parts of concrete cylindrical specimen in the 250x – 25000x

magnification on FEI Quattro S. SEM images were used to analyze the fiber orientation, its clustering and observe its adhesion with cementitious matrix. The SEM images are present in **Fig. 2.**
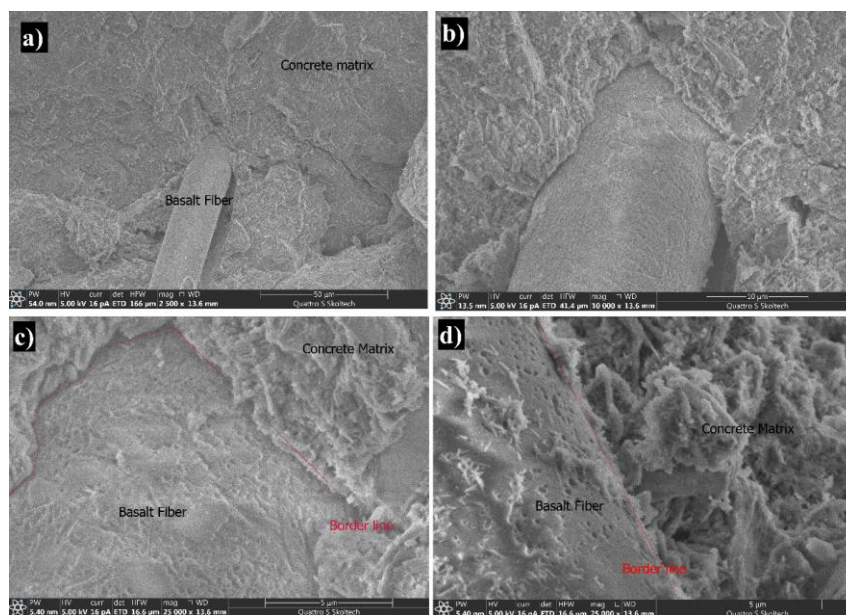

Fig. 2. Adhesion of Basalt Fibers with the Cementitious Concrete Matrix: a) 2500 x - resolution; b) 10000 x - resolution; c) 25 000 x – resolution; d) 25 000 x – resolution.

Two CT scans were acquired before and after low-cycle fatigue tests. The scans were performed of the whole 100x100 mm concrete cylinder on GE Phoenix v|tome L240 with a nanofocus tube, molybdenum detector with 1700x1700 resolution and following scanning parameters: imaging resolution 60 μm/voxel. Using the CT images the following parameters were analysed: average size of CR, pore and CR volume fraction, volume of crack after the experiment. Identification of fiber is not possible on CT due to resolution-size limitations of CT systems. The CT scans are present in **Fig. 3.**
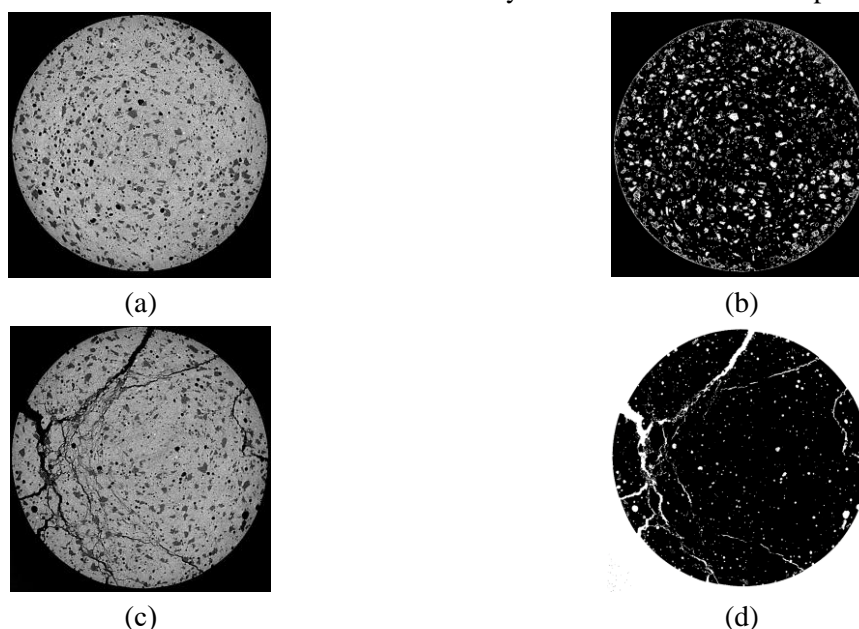

Fig. 3. Procedures for image processing: (a) original slice image file before the experiment; b) Threshold control operation to increase the contrast between the matrix and crumb rubber particles; (c) original slice image file after the experiment; d) Threshold control operation to increase the contrast between the matrix and generated cracks.

The slices are perpendicular in three perpendicular planes. The concrete series' inner structure quantitative characteristics from SEM and CT are demonstrated in **Table 3**.

Table 3. SEM and CT analysis results

Mean equivalent diameter of rubber inclusions, mm	2.5
Rubber volume fraction, %	11.84
Pore volume fraction, %	1.83
Crack volume fraction after the experiment, %	1.92

3 Methodology

Plastic damage and stiffness recovery factors can be described in the damage behaviour of concrete under reciprocating loading, such as stiffness recovery. The relationship between unloading-reloading modulus E_r and damage factor under reciprocating load can be established as:

$$E_r = E_0(1-d) \tag{1}$$

Where d is the damage factor in compression, which ranges from 0 to 1. E_0 – Elasticity modulus.

The unloading-reloading modulus decreases as the damage factor rises due to the concrete's increasing nonlinear behavior [22]. This general damage factor described by equation (1) will be adapted in the VUMAT Plasticity damage model of the concrete material.

Vectorized User Material (VUMAT) plasticity model was developed via FORTRAN and imported into ABAQUS for its validation and seismic analysis of the shear-wall. VUMAT has been developed based on the results acquired from low-cycle fatigue experimental tests for the two consecutive series. The laboratory cyclic tests were performed to characterize energy dissipation and hysteretic damping during cyclic compression with increasing strain amplitudes for the total period of 1000 cycles. To simulate a high intensity earthquake, low-cycle fatigue tests have been performed for high stress, 81-90% of the material compressive strength.

After assembling the VUMAT model in FORTRAN, the model was imported into ABAQUS for Cyclic Pushover Analysis. The problem of seismically-resilient design of the shear wall comes down to an optimal solution demand spectrum for effective damping at performance point of each material as applied to Pushover analysis of the Shear wall. Hysteretic damping and energy dissipating properties laboratory results of two series of the material will be contrasted and explain the results of the Pushover Analysis.

After performing Pushover Analysis, Capacity Spectrum Method [1] is adapted to investigate seismic performance of the shear wall with the focus on the rate of energy dissipation. The principal goal is to contrast two series of material for the optimal performance point for a resilient structural design of the shear wall. This entails determining the ideal hysteretic damping for every series in order to match the maximum deformation capacity. The point at which the base shear drops to 80% of the maximum base shear in the decreasing region of the pushover curve for the shear wall implies the capacity corresponding to a near collapse or collapse-prevention performance level [12]. Before reporting a full set of methods used, an overall procedure for achieving the research aims can be referenced by **Fig. 4.**
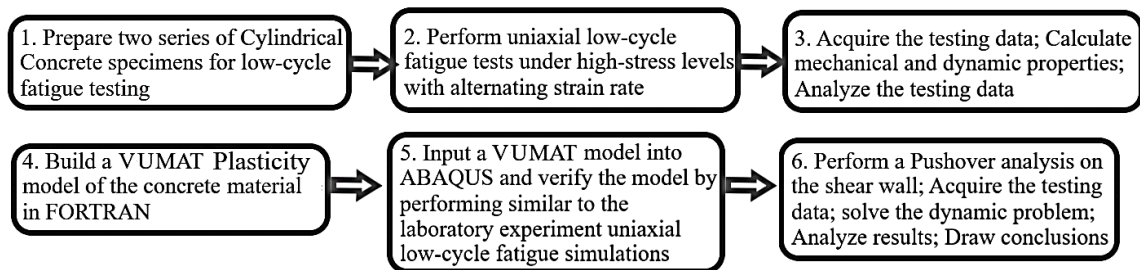
Fig. 4. Research Roadmap.

3.1 Mechanical testing

To investigate energy dissipation, hysteretic damping and associated damage done to a material by inducing high stress-strain levels, low cycle fatigue testing with the total number of 1000 cycles was performed on the specimens of series CR and CRBF per ASTM E606/E606M-21 [27]. Quasi-static

crack extension was considered as a low-cycle fatigue process, discretized to different levels and correlated to the fatigue data. Prior to Cyclic Fatigue testing, according to ASTM C39 [28], uniaxial compression tests were performed for the total number of three specimens per the material series. As a result, Poisson's ratio, Elasticity modulus and compressive yield stress of the concrete two series were determined. The fatigue behaviour of fine-grained rubberized concrete was investigated with respect to the influence of maximum stress level and strain rate on the energy damage evolution and stiffness of the specimens. To simulate a seismic load, investigations were focused on low-cycle-fatigue. Influence of the number of cycles to fatigue failure with consecutive energy dissipation and the developments of strain and stiffness were analyzed.

A specimen was placed in a testing machine between the loading head and the supporting bearing platen (**Fig. 5**). A uniform stress across the specimen's ends was made possible with the help of the bearing platen. The triangular load-control function was utilized to conduct fatigue tests on a servo-hydraulic 25 kN actuator. Key characteristics of the cyclic fatigue testing can be summarized as the following: fatigue failure is the result of N ≤ 1000 number of cycles with high stress levels with alternating strain rates over an extended period that eventually fractures the material and causes failure. These fractures' growth are contrasted between different specimens under different loading states with the correlation to energy dissipation and extrapolated to the structural strength of the shear wall. The used strain rates were 0.1 and 0.05. Loading of a specimen was terminated as soon as the major cracks start to progress in the specimen. Constant amplitude triangular loading was applied (**Fig. 5**). Extensometer was installed on a concrete specimen to measure two perpendicular directions of the specimen deformation.
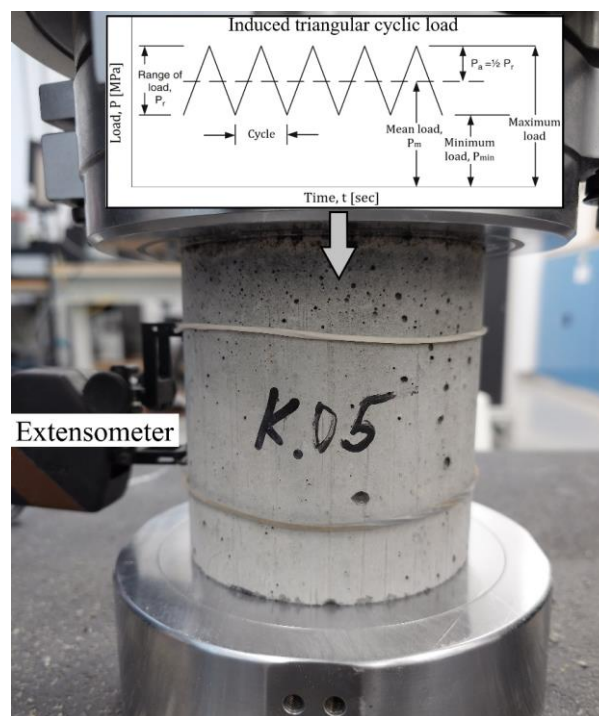

Fig. 5. An experimental setup for a specimen low-cyclic fatigue loading.

3.2 Simulation

3.2.1 Energy Dissipation

The dissipation energy (E_δ) or the term "damping energy" refers to the energy that is absorbed during a loading cycle, transformed, and retained by the specimen or structural element [29]. The total dissipated energy $\sum E_{\delta,i}(N)$ throughout all cycles is accountable for fatigue failure of a specimen. At the same time, during the first loading cycles only the dissipated plastic energy (W_d) is accountable for the predominant damage of a specimen. Dissipated elastic energy (E_{el}) is accountable for the damping

in the material during the subsequent loading cycles. The dissipated energy for one cycle is equal to the decrement of work of the dissipative system during loading and unloading, and can be calculated by finding the area of the hysteresis curve in the "cyclic stress-strain" relation [30,31]:
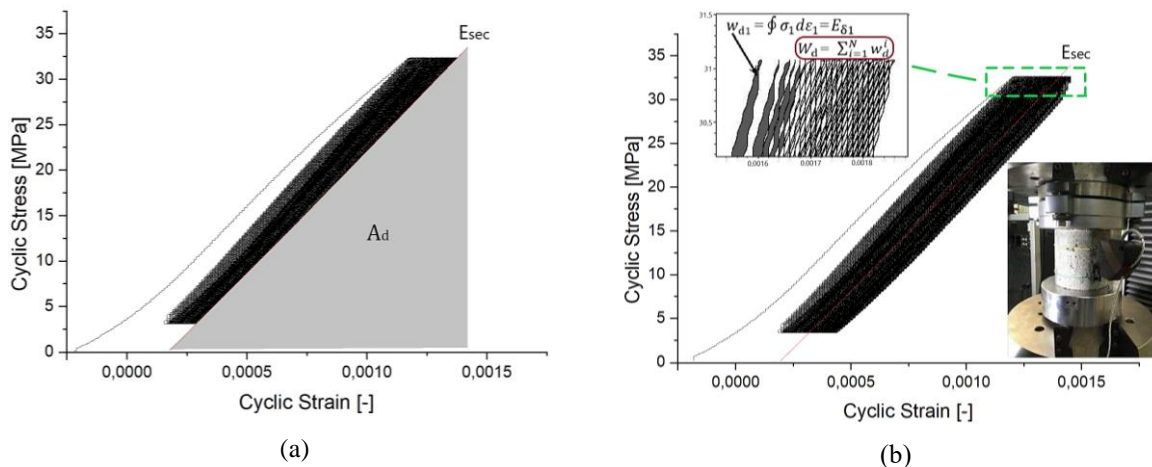

(a)

(b)

Fig. 6. Calculation procedure of Energy-Dissipation Characteristics performed for CRBF-09 specimen: a) Finding ($A_\mathbf{d}$) - elastic strain energy density per cycle; b) Estimation of the dissipated energy ($W_\mathbf{d}$).

By the procedure presented in **Fig. 6**, apart of finding the mentioned above energy-dissipation characteristics, as the parameter of hysteretic damping, damping ratio is calculated as:

$$D_m = \frac{1}{4\pi}\frac{W_d}{A_d} \tag{2}$$

For each applied stress level, the following equations (3-4) are used to calculate the average elastic strain energy density and the dissipated energy density at a point representing elastic strain energy density and the dissipated energy density from the first loading cycle to the current loading cycle n:

$$A_d = E_{el} = \frac{1}{2}\sigma_n\varepsilon_n \tag{3}$$

Due to the additivity of energy, the dissipated energy is defined as the sum of all single-cycle energy dissipations from the initiation of loading to the current cycle N:

$$W_d = \sum_{i=1}^{N} w_d^i \tag{4}$$

Cyclic Energy-dissipation per unit-volume for a concrete cylindrical can be determined [18]:

$$E_{\delta,i,V} = \frac{E_{\delta,i}}{V} = \int_D \sigma_i d\varepsilon_i \tag{5}$$

Where $E_{i,V}$ is the single cycle energy dissipation per unit volume at the ith loading cycle; σ_i is the axial stress applied by testing machine at the ith loading cycle; ε_i is the axial strain measured through extensometer at the i-th loading cycle; V is the volume of a cylindrical specimen; D – the enclosed area of the i-th hysteresis loop; w_d^i - an i-th hysteresis loop under low cycle fatigue experiment of a specimen.

It is important to distinguish the concrete' structural behaviour under consecutive stress-strain conditions and as a result, determine the relationship of crack propagation, secant modulus and the total number of cycles of irreversible crack appearance [32]. The relationship of crack propagation for a given n-th cycle of irreversible crack appear is represented by the parameter:

$$\xi = \frac{E_{\text{sec},c}}{E_0} \tag{6}$$

Where $E_{\mathrm{sec,c}}$ – Secant modulus of a concrete series' i-th unloading curve, E_0- Initial Secant modulus, which is defined as the secant modulus of the first unloading curve.

The irreversible crack propagation is proportional to the amount of the generated cracking energy. Cracking energy can be calculated as:

$$E_{cr,i,V} = \frac{E_{cr,i}}{V} = \int_D \sigma_{cr,i} d\varepsilon_{cr,i} \tag{7}$$

Where $E_{cr,i,V}$ is the total cracking energy of a specimen; $\sigma_{cr,i}$ is the axial stress for a given hysteresis loop that corresponds to irreversible crack generation; $\varepsilon_{cr,i}$ is the axial stress for a given hysteresis loop that corresponds to irreversible crack generation; V is the volume of a cylindrical specimen; D – the enclosed area of the i-th hysteresis loop.

A graphical representation for the cracking energy calculation is shown in the figure below:

3.2.2 VUMAT plasticity model

A plasticity-based global approach is adapted in the model to simulate the nonlinear behaviour of the solid shear wall subjected to high intensity seismic excitation. Concrete evolution of energy damage mechanism describes the plastic strain rate as the concrete degradates and losses its stiffness when subjected to low-cyclic seismic load. Energy damage evolution is identified by an equivalent cyclic law which has been calibrated by a uniaxial approach. The evolution of the internal variables is controlled by rate equations that have a yield surface because that represent irreversible material behaviour [22]. The theory of plasticity defines "when" and "how" the plastic strain occurs [22]. The material assembly can be summarized in three steps as the following:

Step 1: In accordance with the VUMAT notation we can define the material Iso-Elasticity matrix. Deviatoric stresses can be calculated using the mean stress [22].

Step 2: Energy Damage mechanism is defined using a phenomenological approach for energy dissipation evolution: $E_{tot} = E_{el} + E_{pl}$

Where the induced damage fatigue is directly proportional to the dissipated energy in a concrete specimen when subjected to low-cyclic fatigue:

$$E_{pl} = E_{tot} - E_{el} = \sum_{i=1}^{N} E_{\delta,i} \tag{8}$$

Where E_{pl} – plastic energy; E_{el} – elastic energy; $E_{\delta,i}$ – Energy dissipation of a specimen.

Step 3: Then we define the yield surface as a circular cylinder using Von-Mises equivalent stress:

$$\sigma_{\upsilon} = \sqrt{\frac{3}{2} S_{ij} S_{ij}} \tag{9}$$

Then the Energy Damage criterion $D_E(N)$ for a given number of cycles (N) to irreversible crack energy release can be defined as:

$$D_E(N) = \frac{E_{\delta,i}(N)}{E_{fail}(N)} \leq 1 \tag{10}$$

Critical conditions for a specimen fracture, if plasticity has taken place, are defined by Eq. (9) as the equilibrium point at which no net change in total energy occurs and crack growth takes place. The problem then comes down to phenomenological characterization of hysteretic behaviour and energy dissipation rate serves as the experimental variable for a given tested specimen. Its thickness and loading frequency can be determined in an uniaxial low-cycle fatigue test. The occurrence of hysteresis serves as a characteristic of the energy damage criterion. The rationale behind using Von-Mises yield surface is the Von Mises criterion best used to predict the maximum stress that a material can withstand without failing. Henceforth, by incorporating energy damage evolution mechanism with Von Mises criterion we can conduct a computationally efficient simulation of the shear wall that takes into account its full hysteretic behaviour due to the effects of low cycle fatigue.
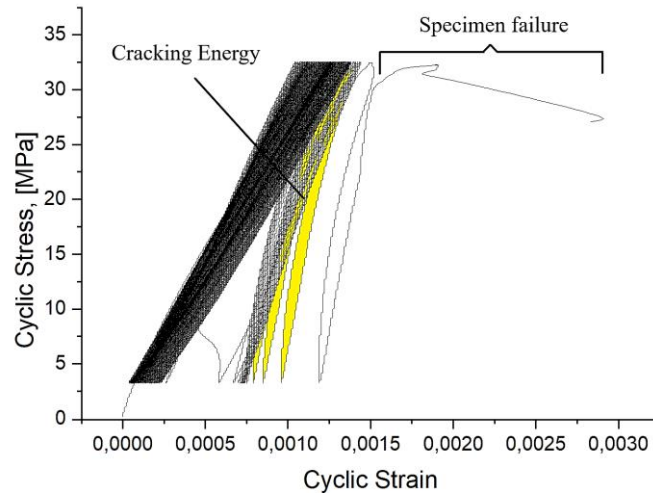
Fig. 7. Calculation of the Cracking Energy for the failed specimen CRBF-05.

3.2.3 Cyclic Pushover Analysis of the Shear Wall

Structural components undergo stiffness and strength deterioration under high magnitude earthquake cyclic loading, which are critical properties of reinforced concrete members under cyclic loading that reduces deformation capacity. With application to four-story buildings, the Cyclic Pushover Method (CPM) is modified to estimate the seismic demands of the solid shear wall [12]. Shear wall design is presented in **Fig. 8**. The dimension of the shear wall are 2650 mm in height, 400 mm in width and 1250 mm in length, respectively.
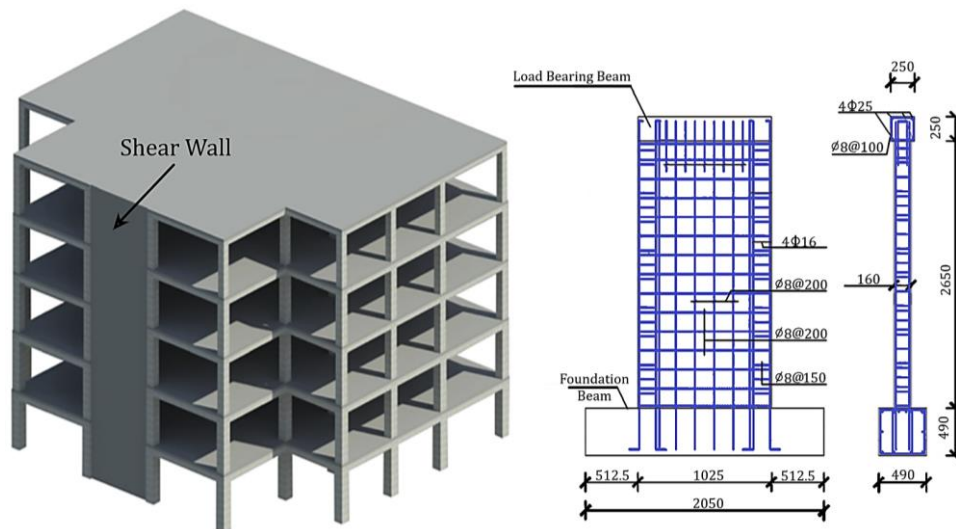
Fig. 8. Design of the Lightweight Shear Wall.

Cyclic Pushover Analysis (CPA) based on the concept of accumulated damage has been initiated to account for the structural stiffness degradation. The models are adapted in the FEA of RC shear-wall to explore the effect of basalt fiber content on the damping and in-structure demand response spectrum. The FE model encompasses shear wall body and foundation assigned as a host to the embedded steel reinforcement. The concrete material paired interaction with the steel reinforcement inside the shear wall is modelled, respectively, so that the seismic behaviour of the concrete series can be properly simulated.

An overall procedure of FE simulations can be summarized by the three main steps as it is shown in the **Fig. 9.** A fundamental assumption adopted in the CPM is that the seismic response of structural elements subjected to earthquake loading can be represented by a curve encompassing the cyclic hysteretic behaviour. Consequently, the structural cyclic load can be used to simulate a seismic excitation from an earthquake. Additionally, throughout the loading period, each structural component

of the simulated shear wall retains a permanent memory of the damages caused by earlier loading cycles, as well as all of the previous excursions that aided in its degradation. As a result, the cumulative damage and the structure's deformation capacities are linked [33]. Nevertheless, this aspect is neglected by the conventional monotonic approaches, which generally overestimate the strength and stiffness of structural members and may lead to an underestimated prediction of the displacement demand [34].

It is now feasible to perform a nonlinear incremental cyclic analysis of the MDOF structure, from which the force-deformation characteristics of the ESDOF system can be established [1]. The resultant of the MDOF structural analysis is a Pushover Curve (capacity curve of the structure) and its corresponding hysteretic behaviour analysis of strength and stiffness degradation (**Fig. 8**). This capacity curve provides a valuable information about hysteretic damping and seismic response of the structure because it approximates how it behaves in the plastic region after exceeding its elastic limit.
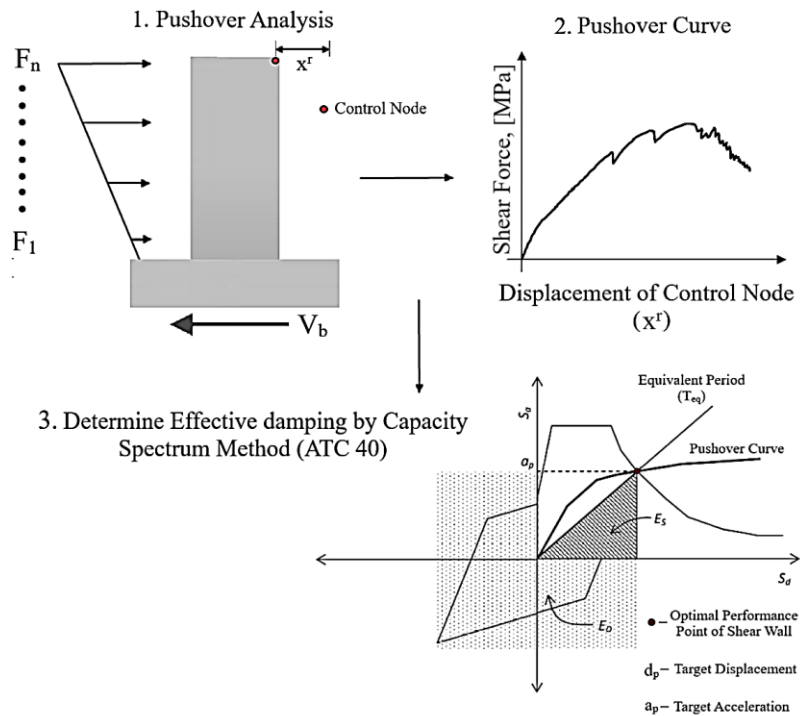

Fig. 9. Graphic Representation for finding an optimal Performance Point by Capacity Spectrum Method (reprinted from **[1]**).

To interconnect a single pushover curve generated by pushover analysis with the demand curve in terms of shear force versus shear displacement, the cyclic response needs to be enveloped by the backbone curve, which is characterised by the cyclic degradation [33].

4 Results and discussions

4.1 Experimental

4.1.1 Material characterization

As it can be seen from **Fig. 2**, adhesion appears acceptable and can be sought as a term for a fine material structural linkage. However, as it is seen from c) and d) – the BF has a rough surface with a considerable amount of pores that can allow the cement pour in and in prospect, provide a less stable structure. These fiber inhomogeneities can be explained by somewhat uneven SEM probe preparation and in reality, other fibers lack those flaws.

Orientation of fibers is contrasted in **Fig. 2** and shows different angles of lining in the cementitious matrix. A visual degree of agglomeration between different cement compounds and the respective CR and BF distributions can be seen in **Fig. 2-3**.

4.1.2 Mechanical Testing

The table below conveys the results of mechanical testing that are used for the VUMAT concrete plasticity model assembly:

Table 4. Results of Mechanical Testing

Parameter	Series CRBF	Series CR
Elasticity modulus (E), [MPa]	25 000 $\pm$ 200	22 000 $\pm$ 200
Poisson's coefficient (v), [-]	0.24 $\pm$ 0.01	0.25 $\pm$ 0.01
Plastic Energy Dissipation (W_d), [kJ]	870 $\pm$ 10	720 $\pm$ 10
Elastic Energy Dissipation (A_d), [kJ]	650 $\pm$ 10	625 $\pm$ 10
Total Energy Dissipation (W_d), [kJ]	1520 $\pm$ 10	1345 $\pm$ 10
Mass Density, (ρ) [tonne/mm^3]	2.09E-09	2,08E-09
Compressive Strength, [MPa]	33 $\pm$ 0.2	31 $\pm$ 0.2

Lateral and axial strain were measured by extensometer. Compressive strength was determined by the testing machine as the maximum allowable stress that a specimen can sustain. Plastic and Elastic energy quantities were obtained by following the procedure of energy dissipation mechanism described in section 3.2.1. A concrete specimen under cyclic load absorbs a certain amount of energy in every consecutive cycle, which is characterized by its hysteresis loop area. Our experiments have demonstrated that the accumulation of fatigue damage is governed by the plastic energy dissipation. Plotting cyclic test data on a stress/strain curve, a concrete specimen exhibiting elastic hysteresis will indicate one path during the loading phase, and a different path during the unloading phase, respectively. The divergence of the two paths occur due to consecutive energy loss in a specimen, with the area between the curves representing the dissipated energy. Total energy continually damages the internal microscopic structure of concrete, which leads to a deterioration in concrete strength and eventually results in a structural failure.
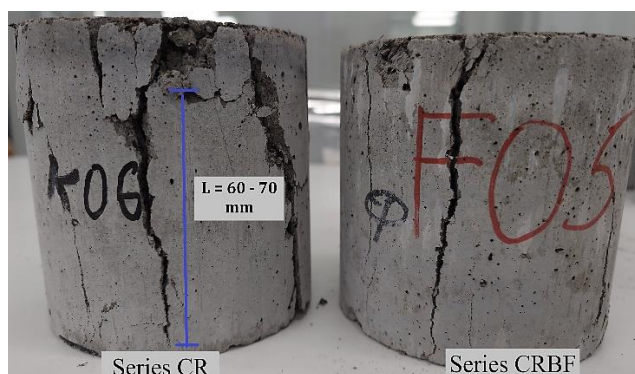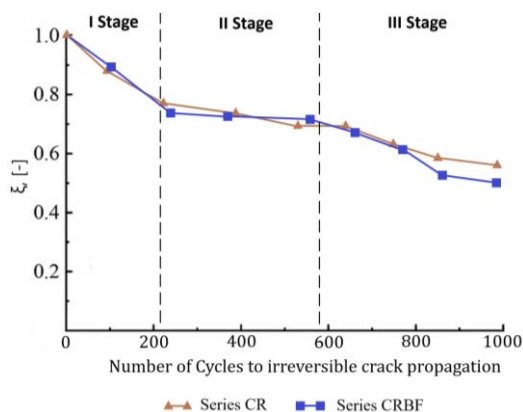

Fig. 10. Crack propagation for the N-th Number of Cycles.

Fig. 10 conveys the trend between parameter ξ and the number of cycles to the occurrence of irreversible crack propagation. As a specimen undergoes a higher range of cycles up to 1000, internal cracks develop more rapidly, in turn resulting in increased damage and a decrease in the secant modulus. The secant modulus has a three-stage degradation law. It rapidly diminishes within 10% of the cycle ratio and decreases slowly in the second stage. The concrete stiffness loss can be calculated as:

$$T_S = 1 - \frac{E_{sec,c}}{E_0} = 1 - \frac{\sigma_{max} - \sigma_{min}}{E_0(\varepsilon_i - \varepsilon_i')}, [\%] \tag{11}$$

As it is observed from **Fig. 11**, the stiffness reduction reaches its peak limit when the cycle counts increases up to 850. The observed evolution of concrete stiffness loss has a typical three-stage fracture process with the fatigue damage variable T_S increasing considerably with a consecutive stress levels growth and loading cycles. This reasoning can be explained using microcrack propagation. As stress levels increase in loading cycles, the propagation rate of microcracks increases, respectively. Hence, it follows that the secant modulus acquired from the final unloading curve is maintained at about 75% of E_0 [35].
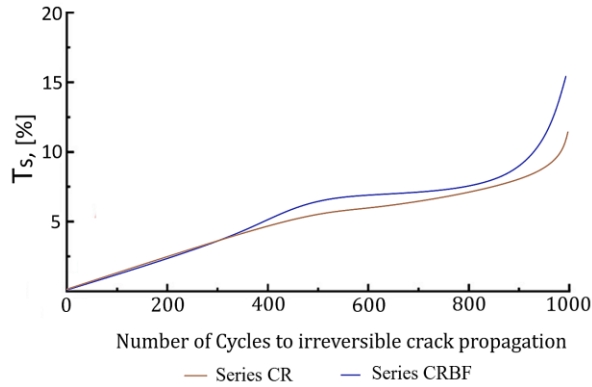
Fig. 11. Stiffness Loss Factor for the N-th Number of Cycles.

4.1.3 Analysis of Energy Evolution

By the process described in **Fig. 6,** the relation between total dissipated energy and the amount of cycles till the specimen failure for each specimen is discussed below. The structural failure criteria for each specimen (**Fig. 12**) represents the total dissipated energy $\sum E_\delta$ for each material specimen at different strain rates throughout the course of cyclic loading and the evaluation of the parameter W_d that mainly involves the assessment of the dissipated energy in the cyclic plastic zone around the crack tip referenced by the methodology in **Fig. 6.**
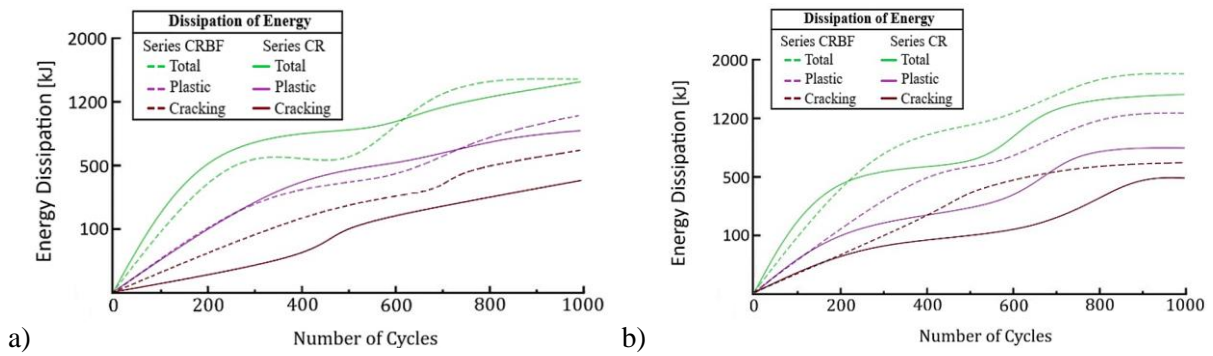
Fig. 12. Characterization of Energy-Dissipation for the series CR & CRBF in: a) 0.1 strain rate; b) 0.05 strain rate.
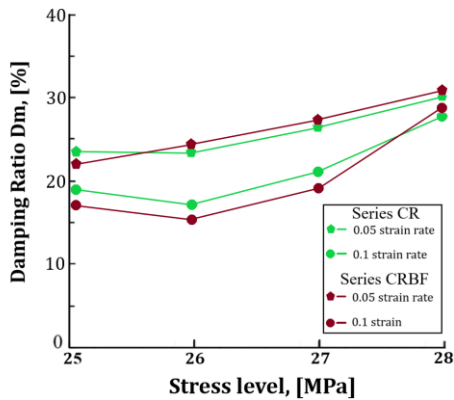

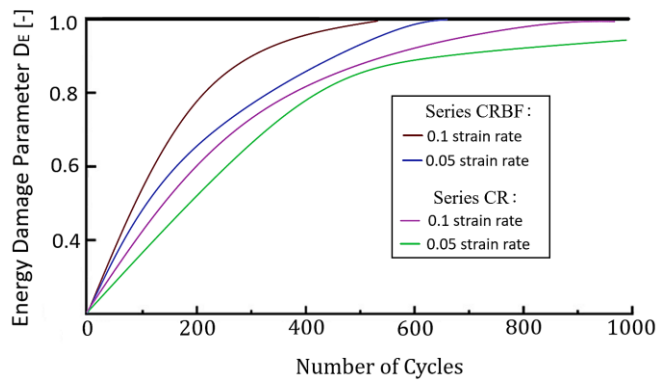**Fig. 13**. Characterization of Damping Ratio at varied stress levels for different strain rates.

Fig. 14. Criterion of structural failure for different strain rates.

The energy dissipation E_δ per loading cycle and the specimens' curves are steeper the fewer loading cycles it takes to reach failure N_F. As a result, it is impossible to predict the incipient failure by defining a critical value or critical gradient of dissipation energy E_δ per loading cycle [29]. By calculating the rate of change between energy dissipation and the number of cycles a specimen has sustained before failure – CRBF series has an 8% faster dissipation rate compared to the CR series. Faster energy dissipation rate employs less prevalent damping characteristics of the CRBF series, which means that

more energy is converted to a potential energy and can be transferred to supporting structural members. With that in mind, it does not yield a negative effect for the reinforced concrete as this energy would be absorbed by steel reinforcement. Characterization of damping ratio for each concrete series at different strain rates is presented in **Fig. 13.**

In summary, a specimen fracture happens when the specimen's total dissipation energy ($\sum E_{\delta,i}$) crosses the "fracture line" as shown in the **Fig. 14**. On this basis, a main criterion of structural failure can be defined as the fracture function $D_E(N)$ per Eq. 10, which depends on the cycle of loading:

The failure criterion D(N) is defined as the ratio of the test series' "fracture line" value, to the specimen's total dissipation energy $\sum E_{\delta,i}(N)$ for each loading cycle N. The cumulative dissipation energy $\sum E_\delta$, and the number of loading cycles to failure N_f from various specimens in the same test series are utilized to determine the failure line $\sum E_{\delta,fail}(N)$. As previously mentioned, the dissipation energy $\sum E_\delta$ per loading cycle and, consequently, the cumulative dissipation energy $\sum E_\delta$ can be computed using only displacement and stress data. Consequently, the energy damage model presented can be used without the need for any extra equipment.

4.2 Mathematical modelling

4.2.1 VUMAT model verification and validation

The model was made based on the cyclic stress-strain data from laboratory uniaxial compression low-cyclic fatigue experiments and consecutive parameters are as described in section 3.3. A summarized material property table for each series of the material is presented in **Table 4**. The list of parameters was averaged for each specimen in the two series, respectively.

Verification of the VUMAT subroutine for simulation of energy-dissipation through explicit cyclic loading is made in contrast to laboratory tests and in-built ABAQUS concrete damage plasticity (CDP) model. Validation of the assembled VUMAT is made based on uniaxial compression cyclic behaviour, time of convergence, and energy-dissipation state under reciprocating cyclic loading.

The relationship between VUMAT validation and model prediction is illustrated in **Figures 15-17**. Model calculations and validation experiments are performed and validated at various strain rates and levels of cyclic stress. The uncertainties in the model output and experimental outcomes can be explained by human factor of experimental work performance. As demonstrated by **Fig. 16**, VUMAT has yielded a more steady convergence for the solution of Energy Dissipation calculation for the lesser amount of computed time. Predictions made at points nearer validation points have higher confidence. The following bar charts show the damping ratio's characterization at various strain rates.
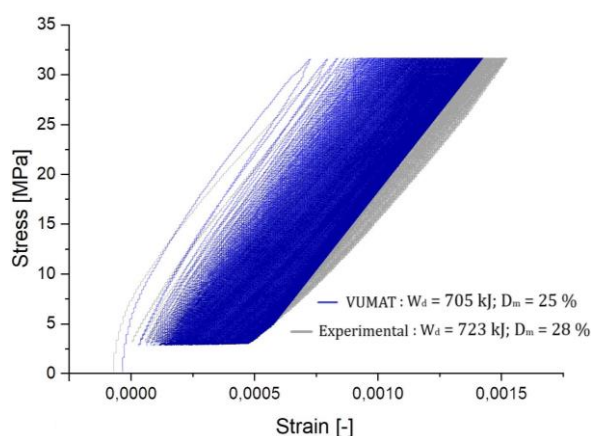

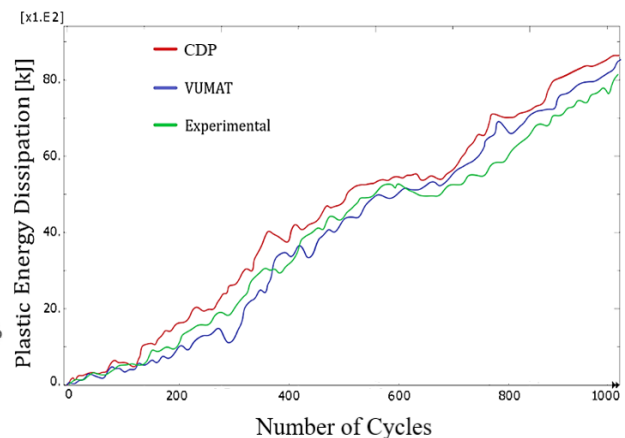**Fig. 15**. VUMAT Verification of the hysteretic behaviour in 0.1 strain rate.

Fig. 16. VUMAT Validation of plastic energy-dissipation in 0.1 strain rate.

4.3 Seismic Response of the Shear Wall

The capacity spectrum method is used to determine the seismic performance level of a shear wall by utilizing target displacement [1]. The seismic demand is represented by the response spectrum curve,

while the pushover curve shows the lateral resistance capacity [1]. The results of monotonic and cyclic pushover analyses are performed such that the structural performance of the shear wall can be directly connected with the concrete VUMAT material constitutive law. Steel material properties were chosen according to the available industrial data and were assigned as presented in **Table 5**.
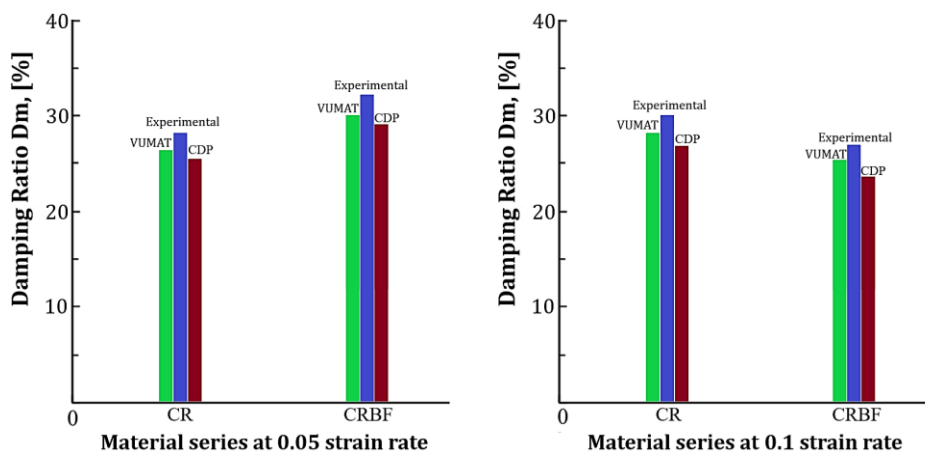

Fig. 17. Characterization of damping ratio for energy-dissipation under consecutive strain rates (0.05-0.1).

Table 5. Steel reinforcement material properties

Parameter	Steel Reinforcement
Young's modulus (E), [MPa]	200 000
Poisson's coefficient (ν), [-]	0.30
Mass Density, (ρ) [tonne/mm^3]	7.8E-09

Plastic behaviour of steel was chosen to follow a kinematic hardening rule with the maximum 520 MPa yield stress. Performance based design response of structure is deployed to take into account the structural behaviour beyond elastic limit. Displacement controlled procedure with the set displacement of 30 mm is applied. **Fig. 18** represents the structural response with the emphasis on the rate of energy-dissipation with the course of time during the pushover analysis. There are two shear wall models that correspond to each concrete material series: SW_CR – shear wall with the concrete series CR and SW_CRBF - the concrete series CRBF.
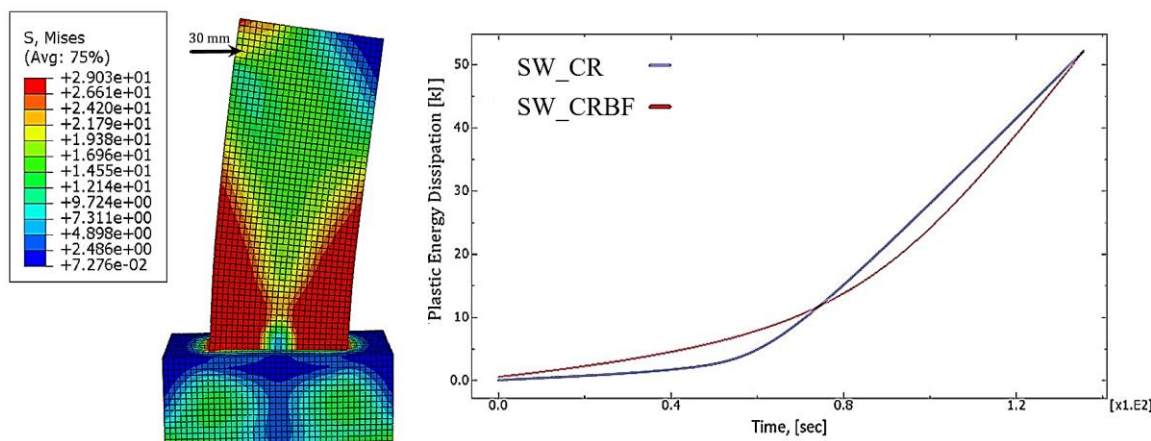

Fig. 18. Convergence of Plastic energy-dissipation for a given model of shear wall.

Three main steps involved in the displacement based response of the shear wall can be summarized in the following three steps:

1. Analysis of each material series' capacity curve, also known as the pushover curve (**Fig. 19**). Examining the base shear distribution in order to calculate the maximum anticipated lateral force on the shear wall's base when it is subjected to seismic excitation is the main goal of this step. 2. Demand curve evaluation, i.e., using cyclic load data to represent earthquake ground motion, and 3. Performance point determination for each shear wall model, which is the point where the demand and capacity curves

intersect (**Fig. 20**). 4. Calculation of energy dissipation from hysteretic loops for each material series in cyclic pushover (**Fig. 20**).
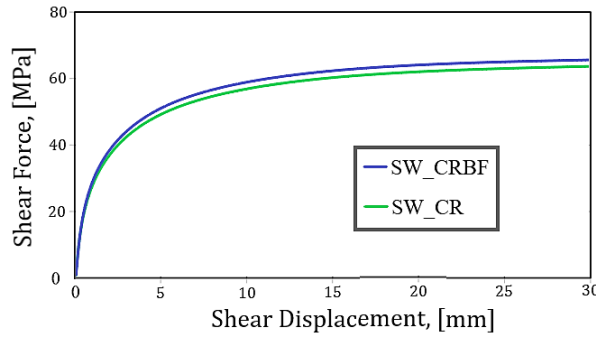

Fig. 19. Capacity curves for two shear wall models corresponding to the series CRBF and CR
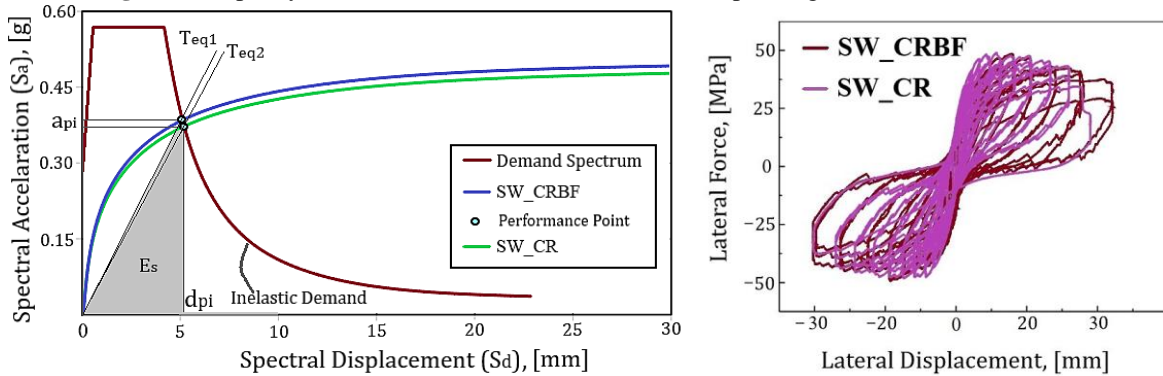

Fig. 20. Capacity Spectrum Method for two shear wall models corresponding to material series CRBF and CR.

At the maximum shear displacement at 30 mm, the maximum shear force equals to 59 MPa for SW_CR and 64.

The inelastic structural behavior under a specific seismic excitation (cyclic amplitude load) is represented by the inelastic demand spectrum. The structure's inherent damping and equivalent viscous damping, which accounts for the energy dissipation of the structure's hysteretic behavior, are represented by the effective damping, as illustrated in **Fig. 20.** The intersection of capacity curve and demand spectrum corresponds to performance point and can be calculated in reference to [1]. Effective periods for two series of the material are computed from the initial period of vibration and from the maximum displacement ductility ratio. Calculation of the hysteretic damping is similar to how the damping ratio (D_m) is computed as $\xi_{hyst} = \dfrac{E_D}{4\pi * E_S}$.

Where E_D- hysteretic energy dissipation that is calculated by finding the area of hysteresis loops generated from a SW model; E_S – maximum strain energy, that can be computed by the area of hatched triangle of stiffness triangle (K_{eq}) formed from finding the points of performance point as $E_S = \dfrac{a_{pi}d_{pi}}{2}$.

The overall resultant variables acquired from the CSM reflect the seismic performance of the shear wall at each performance point for a corresponding SW model are listed in **Table 6**:

Table 6. Performance characteristics of shear wall models

Shear Wall Model	Hysteretic Damping (ξ_{hyst}), [%]	Spectral Acceleration (S_a) [g]	Spectral Displacement (S_d), [mm]	Max Base Shear, [MPa]	Max Displacement at the top, [mm]
CR	8.7	0.395	4.95	59	5.42
CRBF	9.3	0.414	5.43	64	5.35

5 Conclusions

The nonlinear pushover analysis in accordance with ATC-40, has been adapted to characterize hysteretic energy dissipation of shear wall models depending on the concrete series. Structural degradation as subjected to seismic excitation was estimated by the cyclic pushover procedure. For acute characterization of plastic energy dissipation and corresponding energy damage evolution, the VUMAT energy damage plasticity model of concrete has been assembled in contrast to the concrete damage plasticity model. The FE simulations have shown that the shear wall is capable of withstanding the applied seismic loading for both SW material models with 11% differences in energy-dissipation. As a result, BF reinforcement did not provide distinguishing strength, ductility and energy-dissipation for shear wall as subjected to seismic excitation. Nevertheless, the CRBF series has demonstrated better compressive strength than the CR series. The main findings of the research can be summarized in the following manner:

Basalt fiber reinforcement yielded an 8% faster rate of energy-dissipation compared to the CR series. However, the difference is minor and in most cases, the series CR is characterized as the material with larger toughness and a lower rate of crack propagation.

CR series has demonstrated better crack toughness and strength when subjected to high stress low-cyclic fatigue.

FE simulations with the VUMAT energy damage plasticity model have allowed to achieve a 37% reduction in the computation as opposed to the CDP model.

The VUMAT subroutine's simulated hysteretic behavior is more comprehensive than that of the CDP model, making it more suitable for applying to seismic analysis of structures and better describing the hysteretic performance of the reinforced concrete model.

BF' modulus of elasticity is affected by the compressive strength, and there is no significant impact on the damping ratio of rubberized concrete with the addition of basalt fiber.

CRediT authorship contribution statement

All authors contributed to the study conception and design. Material preparation was done by **Evgenii Matiushin** and **Victoria Shvetsova**. Computer Tomography of the prepared specimens was performed by **Alexander Burukhin**. Mechanical Testing was performed by **Stepan Konev**. Data collection and analysis were performed by **Artem Zaitsev**, **Ivan Sergeichev** and **Radmir Karamov**. The first draft of the manuscript was written by **Artem Zaitsev** and all authors commented on previous versions of the manuscript. All authors read and approved the final manuscript.

Conflicts of Interest

The authors declare that they have no known competing financial interests or personal relationships that could have appeared to influence the work reported in this paper.

References

[1] Applied Technology Council. ATC-40: Seismic Evaluation and Retrofit of Concrete Buildings 1996.
[2] Husain M, Eisa AS, Hegazy MM. Strengthening of reinforced concrete shear walls with openings using carbon fiber-reinforced polymers. Int J Adv Struct Eng 2019; 11: 129–50. https://doi.org/10.1007/s40091-019-0216-6.
[3] Lye CQ. Use of recycled and secondary aggregates in concrete: deformation properties. University of Birmingham, 2017.

[4]   Pan L, Hao H, Cui J, Pham TM. Numerical study on dynamic properties of rubberised concrete with different rubber contents. Defence Technology 2023; 24: 228–40. https://doi.org/10.1016/j.dt.2022.04.007.

[5]   Lv J, Zhou T, Du Q, Wu H. Effects of rubber particles on mechanical properties of lightweight aggregate concrete. Construction and Building Materials 2015; 91: 145–9. https://doi.org/10.1016/j.conbuildmat.2015.05.038.

[6]   Najim KB, Hall MR. Mechanical and dynamic properties of self-compacting crumb rubber modified concrete. Construction and Building Materials 2012; 27: 521–30. https://doi.org/10.1016/j.conbuildmat.2011.07.013.

[7]   Ren F, Mo J, Wang Q, Ho JCM. Crumb rubber as partial replacement for fine aggregate in concrete: An overview. Construction and Building Materials 2022; 343: 128049. https://doi.org/10.1016/j.conbuildmat.2022.128049.

[8]   Wang C, Wu H, Li C. Hysteresis and damping properties of steel and polypropylene fiber reinforced recycled aggregate concrete under uniaxial low-cycle loadings. Construction and Building Materials 2022; 319: 126191. https://doi.org/10.1016/j.conbuildmat.2021.126191.

[9]   Wang X, Xia J, Nanayakkara O, Li Y. Properties of high-performance cementitious composites containing recycled rubber crumb. Construction and Building Materials 2017; 156: 1127–36. https://doi.org/10.1016/j.conbuildmat.2017.09.024.

[10]   Wang X, Shao J, Wang J, Ma M, Zhang B. Influence of Basalt Fiber on Mechanical Properties and Microstructure of Rubber Concrete. Sustainability 2022; 14: 12517. https://doi.org/10.3390/su141912517.

[11]   Wu H, Qin X, Huang X, Kaewunruen S. Engineering, Mechanical and Dynamic Properties of Basalt Fiber Reinforced Concrete. Materials 2023; 16: 623. https://doi.org/10.3390/ma16020623.

[12]   Panyakapo P. Cyclic Pushover Analysis procedure to estimate seismic demands for buildings. Engineering Structures 2014; 66: 10–23. https://doi.org/10.1016/j.engstruct.2014.02.001.

[13]   Aliabdo AA, Abd Elmoaty AEM, AbdElbaset MM. Utilization of waste rubber in non-structural applications. Construction and Building Materials 2015; 91: 195–207. https://doi.org/10.1016/j.conbuildmat.2015.05.080.

[14]   Assaggaf RA, Ali MR, Al-Dulaijan SU, Maslehuddin M. Properties of concrete with untreated and treated crumb rubber – A review. Journal of Materials Research and Technology 2021; 11: 1753–98. https://doi.org/10.1016/j.jmrt.2021.02.019.

[15]   Atahan AO, Yücel AÖ. Crumb rubber in concrete: Static and dynamic evaluation. Construction and Building Materials 2012;36:617–22. https://doi.org/10.1016/j.conbuildmat.2012.04.068.

[16]   Kaewunruen S, Li D, Chen Y, Xiang Z. Enhancement of Dynamic Damping in Eco-Friendly Railway Concrete Sleepers Using Waste-Tyre Crumb Rubber. Materials 2018; 11: 1169. https://doi.org/10.3390/ ma11071169.

[17]   Su D, Pang J, Han C, Huang J, Hu X, Shi W. Influence of Basalt/Polypropylene Fiber on Permeability and Uniaxial Compressive Properties of Waste Tire Rubberized Concrete. Materials 2023;16: 481. https://doi.org/10.3390/ma16020481.

[18]   Swaminathan P, Karthikeyan K, Subbaram SR, Sudharsan JS, Abid SR, Murali G, et al. Experimental and Statistical Investigation to Evaluate Impact Strength Variability and Reliability of Preplaced Aggregate Concrete Containing Crumped Rubber and Fibres. Materials 2022; 15: 5156. https://doi.org/10.3390/ma15155156.

[19]   Koulouris A, Limbachiya M, Fried A, Roberts J. Use of recycled aggregate in concrete application: case studies. Sustainable waste management and recycling: Construction demolition waste, Thomas Telford Publishing; 2004; 245–57.

[20]   Calvo FE, Trentacoste ER, Silvente ST. Vegetative growth, yield, and crop water productivity response to different irrigation regimes in high density walnut orchards (Juglans regia L.) in a semi-arid environment in Argentina. Agricultural Water Management 2022; 274: 107969. https://doi.org/10.1016/j.agwat.2022.107969.

[21]   Ragueneau F, La Borderie Ch, Mazars J. Damage model for concrete-like materials coupling cracking and friction, contribution towards structural damping: first uniaxial applications. Mech Cohes-Frict Mater 2000; 5: 607–625. https://doi.org/10.1002/1099-1484(200011)5:8<607::AID-CFM108>3.0.CO;2-K.

[22]   Miramontes D, Merabet O, Reynouard J. Kinematic hardening model based on general plasticity for RC structures. Eleventh world conference on earthquake engineering (UWCEE), 1996; 23–8.

[23]   Osorio E, Bairán JM, Marí AR. Lateral behavior of concrete under uniaxial compressive cyclic loading. Mater Struct 2013; 46: 709–24. https://doi.org/10.1617/s11527-012-9928-9.

[24]   Anya B, Ghosh T. A Study on Effect of Shear Wall in Seismic Analysis of Building. IOP Conf Ser: Earth Environ Sci 2021; 796: 012049. https://doi.org/10.1088/1755-1315/796/1/012049.

[25]   Belén G-F, Fernando M-A, Diego CL, Sindy S-P. Stress–strain relationship in axial compression for concrete using recycled saturated coarse aggregate. Construction and Building Materials 2011; 25: 2335–42. https://doi.org/10.1016/j.conbuildmat.2010.11.031.

[26] Cornejo A, Jiménez S, Barbu LG, Oller S, Oñate E. A unified non-linear energy dissipation-based plastic-damage model for cyclic loading. Computer Methods in Applied Mechanics and Engineering 2022; 400: 115543. https://doi.org/10.1016/j.cma.2022.115543.

[27] E08 Committee. ASTM E606/E606M-21: Test Method for Strain-Controlled Fatigue Testing n.d. https://doi.org/10.1520/E0606_E0606M-21.

[28] C09 Committee. ASTM C39/C39M-18: Specification for Concrete Aggregates n.d. https://doi.org/10.1520/C0033_C0033M-18.

[29] Bode M, Marx S. Energetic damage analysis regarding the fatigue of concrete. Structural Concrete 2021; 22. https://doi.org/10.1002/suco.202000416.

[30] Xie H-P, Ju Y, Li L-Y. Criteria for strength and structural failure of rocks based on energy dissipation and energy release principles. Yanshilixue Yu Gongcheng Xuebao/Chin J Rock Mech Eng 2005; 24: 3003–10.

[31] Sima JF, Roca P, Molins C. Cyclic constitutive model for concrete. Engineering Structures 2008;30:695–706. https://doi.org/10.1016/j.engstruct.2007.05.005.

[32] Jenq YS, Shah SP. A Fracture toughness criterion for concrete. Engineering Fracture Mechanics 1985; 21: 1055–69. https://doi.org/10.1016/0013-7944(85)90009-8.

[33] Barbagallo F, Bosco M, Ghersi A, Marino EM, Rossi PP. Seismic Assessment of Steel MRFs by Cyclic Pushover Analysis. TOBCTJ 2019;13:12–26. https://doi.org/10.2174/18748368019130012.

[34] El Ouni MH, Laissy MY, Ismaeil M, Ben Kahla N. Effect of Shear Walls on the Active Vibration Control of Buildings. Buildings 2018; 8: 164. https://doi.org/10.3390/buildings8110164.

[35] Zhang Q, Wang L. Investigation of stress level on fatigue performance of plain concrete based on energy dissipation method. Construction and Building Materials 2021; 269: 121287. https://doi.org/10.1016/j.conbuildmat.2020.121287.